Nat. Hazards Earth Syst. Sci. Discuss., 3, 1789–1833, 2015
www.nat-hazards-earth-syst-sci-discuss.net/3/1789/2015/
doi:10.5194/nhessd-3-1789-2015

Natural Hazards and Earth System Sciences
Open Access
Discussions

Landslide susceptibility mapping in Mawat area, Kurdistan Region, NE Iraq: a comparison of different statistical models

A. A. Othman[1,2,3], R. Gloaguen[1,3], L. Andreani[1,3], and M. Rahnama[1,3]

[1]Remote Sensing Group, Institute of Geology, TU Bergakademie Freiberg, Bernhard-von-Cotta-Str. 2, 09596 Freiberg, Germany
[2]Iraq Geological Survey, Al-Andalus Square, Baghdad, Iraq
[3]Remote Sensing Group, Helmholtz Institute Freiberg of Resource Technology, Halsbrueckerstr. 34, 09599 Freiberg, Germany

Received: 27 January 2015 – Accepted: 13 February 2015 – Published: 6 March 2015

Correspondence to: A. A. Othman (arsalan-ahmed.othman@student.tu-freiberg.de)

Published by Copernicus Publications on behalf of the European Geosciences Union.

Abstract

During the last decades, expansion of settlements into areas prone to landslides in Iraq has increased the importance of accurate hazard assessment. Susceptibility mapping provides information about hazardous locations and thus helps to potentially prevent infrastructure damage due to mass wasting. The aim of this study is to evaluate and compare frequency ratio (FR), weight of evidence (WOE), logistic regression (LR) and probit regression (PR) approaches in combination with new geomorphological indices to determine the landslide susceptibility index (LSI). We tested these four methods in Mawat area, Kurdistan Region, NE Iraq, where landslides occur frequently. For this purpose, we evaluated 16 geomorphological, geological and environmental predicting factors mainly derived from the advanced spaceborne thermal emission and reflection radiometer (ASTER) satellite. The available reference inventory includes 351 landslides representing a cumulative surface of 3.127 km^2. This reference inventory was mapped from QuickBird data by manual delineation and partly verified by field survey. The areas under curve (AUC) of the receiver operating characteristic (ROC), and relative landslide density (*R* index) show that all models perform similarly and that focus should be put on the careful selection of proxies. The results indicate that the lithology and the slope aspects play major roles for landslide occurrences. Furthermore, this paper demonstrates that using hypsometric integral as a prediction factor instead of slope curvature gives better results and increases the accuracy of the LSI.

1 Introduction

Mass movements such as landslides are one of the most damaging natural hazards in terms of social and economic costs, since they represent a major risk to human life, and private and public properties (Calo et al., 2014; Petley, 2012). Maps of landslides are classified into three classes: inventory maps, density maps, and hazard maps (Guzzetti et al., 2000). Moreover, the landslide investigation can categorized into

NHESSD
3, 1789–1833, 2015

three main groups: (1) landslide recognition, classification, and post-event analysis, (2) landslide monitoring and (3) landslide susceptibility and hazard assessment (Scaioni et al., 2014; Mantovani et al., 1996; Metternicht et al., 2005). Landslide inventory maps represent the spatial distribution of deposition (accumulation) and erosion (triggering) zones produced by a gravity-induced mass movement, which may vary in type, age and activity (Guzzetti et al., 1999). A landslide inventory map can be prepared by different techniques (Guzzetti, 2006). Until now, visual interpretation over aerial photographs and high spatial resolution images with field checking remained the major source and most accurate technique for the preparation of landslide inventory map (Othman and Gloaguen, 2013a). The landslide inventory map is fundamental for producing the landslide susceptibility index (LSI) map (Zhao et al., 2012). The LSI is defined as a probability of the spatial terrain to trigger a landslide over a set of geo-environmental conditions (Ozdemir and Altural, 2013). Such maps are essential for the estimation of potential regions of landsliding (Guzzetti et al., 2005). In addition, the LSI is a fundamental and very useful tool supporting the decision making and planning for land use management (Akgun, 2012).

Over the last decades, many different mapping techniques, such as frequency ratio (FR) (Ozdemir and Altural, 2013; Lee and Talib, 2005; Shahabi et al., 2014), weight of evidence (WoE) (Ozdemir and Altural, 2013; Lee, 2013; Lee et al., 2002a; Tseng et al., 2015), analytical hierarchy process (Shahabi et al., 2014; Ayalew et al., 2005), bivariate statistical analyses (Ayalew et al., 2005; Althuwaynee et al., 2014), artificial neural networks (Lee et al., 2001; Conforti et al., 2014; Qiao et al., 2013; Ercanoglu, 2005; García-Rodríguez and Malpica, 2010), support vector machine (Yao et al., 2008; Peng et al., 2014) and logistic regression (LR) (Ozdemir and Altural, 2013; Shahabi et al., 2014; Lee and Min, 2001; Atkinson and Massari, 1998) have been implemented for the LSI estimation. All these prediction techniques are based on the popular assumption that “the past and the present landslide locations are the key to the future” (Carrara et al., 1995; Capitani et al., 2013a; Zezere, 2002; Van Den Eeckhaut et al., 2006). One can also conclude that the authors assumed that slope failures are determined by landslides controlling factors, and the future slope failures will occur under the same conditions as past slope failures (Lee and Talib, 2005). In addition, the definition of a set of factors that can be used to predict the future occurrences of landslides and to estimate the statistical relationships between the predicting factors for landsliding and the occurrences of landslides is the conceptual knowledge of all LSI techniques (Carrara et al., 1995; Capitani et al., 2013a; Van Den Eeckhaut et al., 2006). The lithology, the slope gradient, the slope aspect, the distance to streams, and to tectonic lineaments are widely accepted as significant factors that are related to the occurrence of landslides (Ozdemir and Altural, 2013; Capitani et al., 2013a; Kayastha et al., 2013; Wang et al., 2013).

In this study, we produced LSI maps for a part of the Iraqi Zagros mountain belt; where no studies of the LSI have been carried out in this area. We selected 16 predicting factors, which play a dominant role in slope stability. These factors are (1) lithology, (2) land cover, (3) slope gradient, (4) slope aspect, (5) slope curvature, (6) plan curvature, (7) profile curvature, (8) hypsometric integral, (9) elevation, (10) drainage density, (11) distance to drainage, (12) distance to lineaments, (13) precipitation, (14) normalized difference vegetation index (NDVI), (15) topographic position index (TPI) and (16) topographic wetness index (TWI). GIS techniques are used to compare between four types of LSI mapping models (FR, WOE, LR and PR) and to evaluate their performances. Where, the PR has never been applied for LSI before.

This study included four main steps: (1) preparation of landslides inventory map based on QuickBird images interpretation, without any consideration of time the occurrences, (2) extraction of the predicting factors for landsliding, (3) selection of four models to produce LSI maps; and (4) performing statistical comparisons between the four examined models.

NHESSD
3, 1789–1833, 2015

2 Study area

2.1 Location

The study area is located between 35°45′ and 36°00′ N and between 45°26′ and 45°35′ E. It comprises the Iraq Zagros Mountains, where mass movements threaten many villages and towns (Othman and Gloaguen, 2013a, b). The studied area covers about 422 km^2, and encompasses part of the Sulaimaniyah Governorate/Kurdistan Region in NE Iraq (Fig. 1). The global landslide hazard distribution (CHRR et al., 2005) shows that the risk of landslide there is between medium and high.

2.2 Geological setting

The Zagros orogenic belt is a part of the Alpine-Himalayan mountain ranges and trends in NW–SE direction. This belt is approximately 2000 km long, extending from SE Turkey through Iraq to southern Iran (Alavi, 1994, 2004). The Iraqi part of the Zagros orogenic belt consists of three main tectonic zones: (1) the Inner Platform (stable shelf), (2) the Outer Platform (unstable shelf), which comprises the Mesopotamia Foredeep, the Foothill Zone, the High Folded Zone, and the Imbricated Zone (IZ); and (3) the Zagros Suture Zone (ZSZ) (Fouad, 2010; Agard et al., 2011; Lawa et al., 2013; Jassim and Goff, 2006) (Fig. 1).

Most of the study area lies within the ZSZ, represented by the Penjween-Walash Zone (PWZ), the Qulqula-Khwarkurk Zone (QKZ), and a small part of the Arabian Outer Platform (unstable shelf) represented by the IZ (Fig. 1). The PWZ is located in the central part of the study area. It consists of ultramafics, gabbro, metabasalt, conglomerates, sandstones, marbles, calc-schists, volcanic basalt and andesite. The QKZ is located in the northeastern part of the study area. It consists of radiolarian mudstone, chert, limestone and pebbly conglomerate rocks. The IZ is located in the southwestern part of the study area. It includes three formations, which are composed mainly of limestones, calcareous sandstones, marls, mudstones, shales, and conglomerates.

NHESSD
3, 1789–1833, 2015

Two main thrust faults clearly mark the upper and lower contacts of the PWZ. The two thrusted sheets have steep slopes, folds of chevron type, and contain boudinage structure. The area formed during the Late Cretaceous and Mio-Pliocene periods (Jassim and Goff, 2006; Smirnov and Nelidov, 1962; Al-Mehaidi, 1974; Buday and Suk, 1978; Ma'ala, 2008).

2.3 Climate

Mawat area is characterized by annual variations in precipitation, temperature and evaporation. It has dry summers and wet winters (Fig. 2). The entire annual precipitation (896 mm) occurs from October to May. The highest precipitation is in January with an average value of 199.6 mm. Monthly temperatures range between –2.1 °C (January) and 37.3 °C (August). The snowfalls occur for > 10 days yr^{-1} on average between November and April. Heavy snowfall and rapid snow melting lead to the incidence of landsliding in Mawat area.

2.4 Landslides

The study area has frequent landsliding because of environmental and/or human-induced reasons (Fig. 3). The very rugged topography inducing strong variations in the slope, the altitude, the heavy rainfalls, the rapid snow melting especially in spring, and the relatively heterogeneous geology and geomorphology are the main natural factors of mass movements. Civil engineering activities like road cuts, overloading of the top or undercutting of the toe of slopes are the main Human-induced factors (Othman and Gloaguen, 2013a; Sissakian et al., 2004).

Othman and Gloaguen (2013a) prepared an inventory map of 351 landslides of the study area by compiling one existing 1 : 100 000 scale geological map (Buday and Suk, 1978), visual interpretations of QuickBird imagery and field surveys. The landslide boundaries were identified with high certainty from the QuickBird data based on attributes such as texture, tone, headwall scarps, associations like fragments of transferred materials, and the pathway of these materials. The total landslides coverage accounted for an area of 3127 km^2. The detected landslide size varied from 16 m^2 to 0.32 km^2 (Othman and Gloaguen, 2013a).

For instance, along the main road to Gimo Mountain, after Kanaro village, landslides have affected large areas. Recent events caused road blockings and several towns nearby are threatened and regularly affected. A large rock fall was witnessed recently to the north of Chowarta town (Fig. 3).

3 Methodology

3.1 Material

The ASTER sensor has 14 bands including Nadir (N) and backward looking (B) (0.76–0.86 µm) for the third band. ASTER scene covers 60 km × 60 km on land (Abrams and Hook, 2001). The ASTER level 1A system scene of 15 m resolution was orthorectified and acquired on 24 August 2003. Moreover, four cloud-free QuickBird scenes were used. The scenes were acquired on 29 August 2006 via Ministry of Planning (Iraq). The scenes are orthorectified, radiometrically corrected, and projected using the WGS84 datum and the UTM 38N projection. The final product is an 8-bit, 0.6 m spatial resolution, and comprises of three visible spectral bands; blue (0.45 to 0.52 µm), green (0.52 to 0.6 µm) and red (0.63 to 0.69 µm) (DigitalGlobe, 2006).

ENVI (Environment for Visualizing Images) software was used to perform the data operations. Lineaments were extracted automatically from Digital Elevation Model (DEM) using a MATLAB based toolbox called TecLines software (Rahnama and Gloaguen, 2014b, a). The hypsometric index and the drainage network were extracted using the MATLAB-based software TecDEM (Shahzad and Gloaguen, 2011). Additional GIS operations (Slope, Aspect, curvature, plan curvature, profile curvature, topographic wetness index, density map, distance map, interpolation and base map preparation) and the final map preparation were performed using ArcGIS10 (ESRI, 2011). Statistical analyses were conducted using R-based scripts.

3.2 Input and preparing parameters

There is no agreement on which predictive factors have to be used in LSI analyses, but most of existing works evaluated topographical, geological and environmental factors as essential predictive factors (Nefeslioglu et al., 2008a). Sixteen predictive factors of landslides prepared, and stored as thematic maps. These factors are classified into three categories: geomorphological, geological, and environmental factors. We reclassified these thematic factor maps to have a similar pixel size of ASTER DEM, i.e. a 15 m spatial resolution.

The input parameters have two forms: discrete and continuous. The discrete form (group A) includes lithology, land cover and slope aspect, while the rest (group B) are continuous forms. We prepared the input parameters in two ways based on the applied model. The first way is used for FR and WOE models while the second one is used for LR and PR models. The FR and WOE models are only able to test input parameters that have discrete form (Schicker and Moon, 2012). Therefore, we classified each factor of group B into several classes to be in a discrete form like group A. The LR and PR models are able to test input parameters that have both discrete and continuous forms (Choi et al., 2012), but the discrete form should be binary. Therefore, we binarized each factor of group A, where the target class has a digital number "one" and the rest of the classes are zero. Finally, each discrete factors form generated a number of binary maps an equal the number of the classes of the factor itself (e.g. the lithological map, which has 9 classes' generated 9 binary maps).

3.2.1 Geomorphological factors

We used the following eight factors as geomorphological predictive factors of landsliding: (1) elevation (DEM) which is an important factor causing the landslides (Ozdemir

NHESSD
3, 1789–1833, 2015

and Altural, 2013; Wang et al., 2013; Xu et al., 2012). It is extracted from Nadir (N) and backward looking (3B) bands of ASTER data. The elevation is used to extract the rest of the geomorphological parameters. (2) Slope gradient, which is the major factor of slope stability analysis (Lee and Min, 2001; Yalcin et al., 2011). (3) Slope aspect can be defined as a downslope direction. It control the predictive factors of the occurrence of landslides such as the exposure to sunlight, winds, rainfall (Yalcin et al., 2011), and vegetation cover (Garcia-Rodriguez et al., 2008). (4) Slope curvature represents a line created by the intersection of a random plane with the land surface (Nefeslioglu et al., 2008b). (5) Profile curvature and (6) Plan curvature are the curvature of the surface in the direction and perpendicular of the maximum slope, respectively (Moore et al., 1991). For plan, profile and slope curvatures, a positive curvature refer to upwardly convex surface of that cell. A negative curvature refers to the upwardly concave surface of that cell. A value of 0 refers to flat surface (Xu et al., 2012; Mancini et al., 2010). These parameters were derived using 3×3 moving windows in standard ArcGIS tools (ESRI, 2012). (7) Hypsometric integral (HI) is an appropriate index to identify the evolutionary stage of landscape development (Othman and Gloaguen, 2013b; Strahler, 1952; Perez-Pena et al., 2009). Only Lin et al. (2011) used this index as one of predictive factors when they mapped the landslide susceptibility map in Taiwan. HI above 0.6 indicates elevated landscapes with an entrenched drainage network. HI between 0.35 and 0.6 corresponds to significantly eroded areas with a developed system of V-shaped valleys. HI below 0.35 indicates relatively flat landscapes with a low degree of incision (Strahler, 1952). As the HI value is sensitive to erosion (Perez-Pena et al., 2009), we used a moving window with 100 pixels representing ~ 1.5 km to create the HI map using the TecDEM software. According to Pike and Wilson (1971) the HI can be approximated by the following Eq. (1):

$$\mathrm{TPI} = \frac{\mathrm{Elevation}_{\mathrm{mean}} - \mathrm{Elevation}_{\mathrm{minimum}}}{\mathrm{Elevation}_{\mathrm{maximum}} - \mathrm{Elevation}_{\mathrm{minimum}}}. \tag{1}$$

In this study, (8) Topographic position index (TPI) used for the first time as a predictive factor. It measures the variation between elevation at the central pixel (E_C) and the average elevation (E_A) around it, within a predetermined matrix length (M). The TPI Eqs. (2) and (3) (De Reu et al., 2013; Weiss, 2001) is:

$$\mathrm{HI} = E_C - E_A \tag{2}$$

$$E_A = \frac{1}{n_M} \sum_{i \in m} E_i. \tag{3}$$

Negative TPI values indicate that the central pixel is situated lower than its average surroundings; while positive TPI values indicate that the central pixel is located higher than the average. We implemented a script in the TecDEM toolbox in order to compute the TPI for the studied area. We used a moving window of 100 pixels (~ 1.5 km).

3.2.2 Geological factors

Lithological and structural variations lead to variation in strength and stability of materials (Ayalew and Yamagishi, 2005). We thus used two geological factors as input parameters: (1) lithology (2) distance to lineaments. The lithological map of Mawat area involves eight lithological units (Othman and Gloaguen, 2014).

Many faults are not mapped in the previous geological maps. Therefore, we mapped the lineaments using TecLines (Rahnama and Gloaguen, 2014b), which allows the extraction of image discontinuities from DEM. The DEM was resampled to a resolution of 900 m in order to avoid noisy image discontinuities. The final lineaments are exported to a shape file. We computed the density of tectonic lineaments and distance to tectonic lineaments which are frequently used to map landslides susceptibility (Capitani et al., 2013a, b; Choi et al., 2012; Pradhan et al., 2006).

3.2.3 Environmental factors

Six parameters are defined as environmental predictive factors of landsliding: (1) land cover map, with eight classes provided by GEOSURV-Iraq (Al-Rubaiay and Al-Dulaimi, 2012). (2) Precipitation map, constructed using the climatological stations located within and surrounding the study area. These daily short-time data span for a period of 7 years (2000–2006). The precipitation data is interpolated using inverse distance weighted (IDW) algorithm to create an average annual precipitation map. (3) Increase in the landslides frequency is related to lack of appropriate vegetation cover (Othman and Gloaguen, 2013a; Shahabi et al., 2014). Therefore, the normalized difference vegetation index (NDVI) was calculated (Rouse et al., 1974) after extraction of the reflectance (ρ) from the digital number (DN) of ASTER VNIR data level 1A.

Drainage network analysis is a robust tool to investigate landslides, as there is a relationship between the landslide area and rivers (Othman and Gloaguen, 2013b). (4) Drainage density was derived from the drainage networks around the central point within a predetermined radius of 3000 m. Buffers surrounding the drainage are used to calculate (5) the distance to drainage. (6) TWI is used to study spatial scale effects on hydrological processes. It is a landslide predicting factor related to the runoff (Beven and Kirkby, 1979). TWI is defined as Eq. (4) (Beven and Kirkby, 1979).

$$\mathrm{TWI} = \ln \frac{A_\mathrm{S}}{\tan\theta} \tag{4}$$

where TWI is topographic wetness index for each pixel, θ is the slope angle (°) and A_S is the catchment area (m), which computed using ArcGIS.

3.3 Landslide susceptibility models

The resulting accuracy of the LSI mapping depends on the data quality and mapping model (Chen et al., 2013). In this study, the spatial relationship between landslide locations and each predicting factor for landsliding was derived using FR, WOE, LR and PR models. These four statistical models were used to map the LSI.

NHESSD
3, 1789–1833, 2015

3.3.1 Frequency ratio (FR)

FR represents a simple and common model to generate the LSI map (Ozdemir and Altural, 2013; Lepore et al., 2012; Lee and Talib, 2005; Shahabi et al., 2014; Park et al., 2013; Mohammady et al., 2012). We assigned the LSI for each unit cell in the study area using FR model by implementing the Eqs. (5) and (6) (Wang et al., 2013; Lepore et al., 2012; Regmi et al., 2010).

$$\mathrm{FR}_j = \frac{\mathrm{Al}_i/\mathrm{Al}}{\mathrm{Ac}_i/A} \tag{5}$$

$$\mathrm{LSI} = \sum_{j=1}^{n} \mathrm{FR}_j \tag{6}$$

where Al_i is the number of landslides cells of the category (i), Al is the total number of landslides cells, Ac_i is the number of cells of the category (i), A is the number of cells of the study area, FR_j is the FR value for the chosen class of factor j, n is the total number of factors included in the study (here $n = 15$) and LSI is the LSI based on the FR. FR_j magnitude > 1 means high probability of landslide occurrence, whereas $\mathrm{FR}_j < 1$ means low probability of landslide occurrence (Ozdemir and Altural, 2013; Shahabi et al., 2014).

3.3.2 Weight of evidence (WOE)

The Bayesian probability model, known as the WOE. It is clearly described by Lee et al. (2002b), Regmi et al. (2010) and Meyer et al. (2014). In summary, positive weights (W^+) and negative weights (W^-) are estimated based on the presence or absence of the landslides within the area for the classes of the predicting factors by using the following Eqs. (7) and (8); (Van Den Eeckhaut et al., 2009).

NHESSD

3, 1789–1833, 2015

Landslide susceptibility mapping in Mawat area, Kurdistan Region, NE Iraq

A. A. Othman et al.

$$W^+ = \ln\left[\frac{\mathrm{Al}_i/\mathrm{Al}}{\mathrm{Ac}_i/A}\right] \tag{7}$$

$$W^- = \ln\left[\frac{1-(\mathrm{Al}_i/\mathrm{Al})}{1-(\mathrm{Ac}_i/A_O)}\right] \tag{8}$$

where, Al_i is the number of landslides cells of the category (i), Al is a total number of landslides cells, Ac_i is the number of cells of the category (i), A_o is the number of cells outside the landslides i.e. number of study area cells minus total number of landslides cells. The weight contrast (C) represents the difference between the W^+ and W^- (Eq. 9; Mohammady et al., 2012; Meyer et al., 2014), the magnitude of the contrast reflects the overall factor association between predicting factors for landsliding and landslides (Ozdemir and Altural, 2013; Mohammady et al., 2012; Meyer et al., 2014). A negative contrast indicates a negative spatial correlation, and vice versa for a positive contrast (Ozdemir and Altural, 2013; Corsini et al., 2009). The final probability (P) for each cell is the sum of the weights of each predicting factor for landsliding and the prior probability ($P_{\mathrm{p(s)}}$) (Eq. 10; Ozdemir and Altural, 2013). The prior probability ($P_{\mathrm{p(s)}}$) is given by (Eq. 11; Ozdemir and Altural, 2013).

$$C = W^+ - W^- \tag{9}$$

$$P = \exp\left(\sum W^+ + \ln P_{\mathrm{p(s)}}\right) \tag{10}$$

$$P_{\mathrm{p(s)}} = \frac{\text{Number of landslide cells}}{\text{Number of total study area cells}} \tag{11}$$

3.3.3 Logistic regression (LR)

In this work, we applied the logistic regression, which is one of the multivariate statistical regressions. This model has been widely applied for LSI mapping (Guzzetti et al., 1999). The resulting analysis range is between one and zero, which measures the presence or absence of the landslides, respectively (Althuwaynee et al., 2014). The LR can be expressed in the following Eqs. (12) and (13) (Kleinbaum and Klein, 2011):

$$P = \frac{1}{1 + e^{-z}} \tag{12}$$

$$z = \alpha + \beta_1 X_1 + \beta_2 X_2 + \ldots + \beta_n X_n \tag{13}$$

where α is the intercept of the model, n is the number of variables, β are the beta values associated with each of the independent variables, P is the probability which varies between 0 and 1 on an S-shaped curve and z varies from $-\infty$ to $+\infty$ on an S-shaped curve.

3.3.4 Probit regression (PR)

We performed a probit regression, which is a binomial statistical regressions. The probit link function represents the inverse of the cumulative distribution function of the standard normal distribution to transform probabilities to the standard normal variable. The formulas (Eqs. 14 and 15) of this model are (Aldrich and Nelson, 1984; McCullagh and Nelder, 1983):

$$z = \Phi^{-1} P \tag{14}$$

$$\Phi(z) = \frac{1}{\sqrt{2\pi}} \int_0^z \exp\left(\frac{-t^2}{2}\right) \mathrm{d}t \tag{15}$$

where Φ denotes the cumulative normal distribution function, P represents the probability and varies between 0 and 1, and z varies from $-\infty$ to $+\infty$ and can be calculated using Eq. (13).

NHESSD
3, 1789–1833, 2015

3.4 Preparation of training dataset

We used the inventory map produced by Othman and Gloaguen (2013a). We classified the boundaries of landslides into two zones and digitized: (i) the landslide triggering zone and (ii) the landslide accumulation zone. The geometrical attributes are stored in a GIS database as a shape file and then converted to raster of 15 m resolution. Only the triggering zone of the landslides is included in the susceptibility analysis (Atkinson and Massari, 1998; Van Den Eeckhaut et al., 2006; Thiery et al., 2007). Following the suggestions in many literatures (Bai et al., 2012; Xu et al., 2012; Erener and Duzgun, 2012), we sub-divided the landslides randomly into training and validation data subsets. The training dataset included 80 % of the pixels (11 137 landslide-present pixels), and the validation set included the remaining 20 % of the pixels.

We used this 80 % (~ 0.3 % of the total study area) as training dataset to calculate the LSI of FR and WoE. The LR and PR models need not only landslide-present pixels, but also landslide-absent training dataset to estimate the LSI (Ozdemir and Altural, 2013; Ayalew and Yamagishi, 2005). Therefore, we randomly selected a landslide-absent pixels datasets that include same number of landslide-present pixels. The present study includes 11 137 landslide-present pixels and 11 597 landslide-absent pixels. The predicted factors represent the independent variables while the class values (landslide-present and landslide-absent) i.e. 0 and 1 are the dependent variable. The pixels that have all information of the predictive factors were exported and saved as a text file. This file was analyzed using R software to obtain the estimation constants (α and β), which are important for calculating z.

3.5 Models validation

We used two validation methods to recognize the best susceptibility map model. The first is a quantitative measurement called the areas under curve (AUC) of the receiver operating characteristic (ROC). The AUC is widely used to estimate the accuracy of LSI models (Yesilnacar and Topal, 2005). An ROC curve is a two-dimensional plot.

NHESSD
3, 1789–1833, 2015

The x axis is LSI rank (%) and the y axis is cumulative percentage of validation landslide occurrence (%). An acceptable model should have an AUC of more than 50 % (Fawcett, 2006). The second validation approach is R index (Santacana et al., 2003; Baeza and Corominas, 2001; Schicker and Moon, 2012). It represents a ratio between the area of landslides in the class as a percentage of all landslides area and the susceptibility class as a percentage of the total area (Eq. 16). The spatial distributions of the LSI values given by four models are classified in ArcGIS software into five susceptibility classes: very high, high, moderate, low and safe using natural breaks technique (Ozdemir and Altural, 2013; Shahabi et al., 2014; Mărgărint et al., 2013; Intarawichian and Dasananda, 2011; Poli and Sterlacchini, 2007). The natural breaks give good results when the LSI histogram shows evident breaks (Mărgărint et al., 2013). The best model has highest AUC and R index value of very high and high classes.

$$R \text{ index} = \left(\frac{\left(\frac{n_i}{N_i}\right)}{\sum \left(\frac{n_i}{N_i}\right)} \right) \cdot 100 \tag{16}$$

where n_i is the area of landslides in susceptibility class i, N_i = area occupied of susceptibility class i.

4 Results

4.1 Predictive factors

The extracted elevation ranges from 663 to 2360 m (Fig. 4a), where the highest area is located in the east of the study area. More than 45 % of the landslides are located in the range of 900–1300 m, and 34 % of them are between 1500–1900 m. The TPI ranges from −258 to 406 m (Fig. 4b). In TPI map, 70 % of the landslides occur in a zone of −65–100 m. The slope aspect includes nine faces, which are flat, north, northeast, east, southeast, south, southwest, west, and northwest (Fig. 4a). 64 % of the landslides faced north to east direction. The maximum slope gradient is 65. The result shows that about 82 % of the landslides occur when the slope is between 10 to 35° (Fig. 4d; Table A1). The HI is between 0.1–0.7 (Fig. 4e), and 86.5 % of landslides occur in the range 0.35–0.6 (mature phase). Curvature map has a range between (−41.78) and 49.78 (Fig. 4f),the plan curvature has a range between (−25.79) and 26.48 and the profile curvature has a range between (−26.76) and 21.86 and there is no clear relation of landslide distribution and the type of curvatures. Only curvature, plan and profile curvature have high correlation (more than 0.85) with each other, therefore we used only the curvature as a prediction factor (Fig. 4f).

The study area consists of different lithostratigraphic units. Mawat area has been subdivided by Othman and Gloaguen (2014) into eight lithological classes, (1) ultramafic (2) gabbro (3) metabasalt and basalt (4) gabbro to diorite with ultramafic inclusions (5) limestone, marble, calc-schist and clastics (6) clastics (7) conglomerate and (8) floodplain and valley fill sediments (Fig. 5a). The limestone, metabasalt and clastic rocks consist of 83 % of the total area of the landslides. The farthest point in the study area from the image discontinuities is 2856 m (Fig. 5b). The buffering zone within 450 m from image discontinuities collect about 68 % of the published fault map (Fig. 5a) (Al-Mehaidi, 1974). The distribution of the landslides has been studied in relation to the existence of image discontinuities in the whole of the study area. The areas that are closer than 1000 m to the image discontinuities collect 96 % of the landslides (Fig. 5b).

The maximum TWI reaches 19 (Fig. 6a), and TWI between 6 and 9 comprise more than 54 % of the landslides. The NDVI ranges from −0.12 to 0.75. 92 % of the landslides occur in non-vegetated areas with NDVI values smaller 0.22 (Fig. 6b). Eight classes of land cover are existing in the study area; these are urban and built-up land, vegetated land, cultivated land, burn land, harvested land, igneous and/or metamorphic rocks, and sedimentary rocks. The majority of the landslides occur in sedimentary and igneous rock of land cover classes (Fig. 6c). The annual precipitation range is 763–896 mm; it increases from SE towards NW of the study area. The class of < 833 mm

NHESSD
3, 1789–1833, 2015

has 45 % of total landslides, although the area of this class covers 25 % of total study area (Fig. 6d). The drainage density range from 0.58–2.64 and the farthest point in the map area from the drainage is 936 m (Fig. 6e). It is very clear that the areas with moderate drainage density involve landslides more than the areas with low and high drainage density. The highest density of landslides have a distance from 300 to 400 m from the drainage (Fig. 6f). We classified all above-mentioned factors to use them in FR and WoE models (Table A1).

4.2 Landslide susceptibility assessment

The LSI maps have been prepared using four different models. We evaluated the predictive factors qualitatively to select influencing factors and to enhance the prediction accuracy of the LSI map.

4.2.1 Landslide susceptibility assessment using frequency ratio and weight of evidence

The relationships between landslides and landslide prediction factors using FR and WoE models are shown in Table A1. Precipitation classes show that the < 833 mm class has highest value of FR of 1.82 and C weight of 0.911 (Table A1). In the lithological classes, the gabbro to diorite class has higher FR of 2.195 and C of 0.795 than the clastic rocks class, which has FR of 1.799, and C of 0.617. The harvested land FR is 1.353 and C is 0.340, indicating a high probability of landslide occurrence. The highest value of FR 2.118 and C 0.869 are distributed at elevations between 1701 and 1900 m. The highest FR value of 1.399 and C 0.426 are represented areas that have slopes between 15 and 20. Assessment of distance to lineaments show that distances of 750–1000 m with FR 1.287 and C 0.285 weights have high correlation with landslide occurrence. In the case of distance to drainage, the distance between 300 and 400 m has FR and C weight of 1.322 and 0.314, respectively. In terms of drainage density,

NHESSD
3, 1789–1833, 2015

landslides were most abundant between 1.25 to1.55 densities, where the weight of FR is 1.534 and the weight of C is 0.522.

In the case of aspect, most landslides occurred facing northeast and east where the weight of FE is > 2, and the weight of C is > 0.86. In the case of hypsometric integral, higher FR and C weight are 1.705 and 0.769, respectively, which are found in 0.35–0.425 class. Relation between TWI and highest landslide probability show that the TWI class > 10 has FR 1.205 and C 0.214. Similarly, FR value is 1.123 and C is 0.152 for TPI < −65. FR values decrease with the NDVI in the study area. The 0.12–0.15 class has the higher FR weight of 1.268 while the C weight is 0.333 (Table A1).

We tested more than 10 various combinations of prediction factors for each of FR and WoE to select the better model of prediction factors. The factors that show low correlations are given highest accuracy were determined experimentally. The final FR and WoE maps were calculated from only 12 factors. The ranges of the prediction factors are good indicator to their effect. Figure 7a shows that the lithology, the slope aspect and the elevation have more effect than other factors in the WoE models, while the WoE model is more sensitive to lithology, hypsometric integral and slope aspect factors. Curvature and land cover are not considered as they contributed negatively to the model output by decreasing the AUC of ROC. The LSI map has been classified by equal areas and grouped into five classes with frequency levels of 20, 40, 60, and 80 %. These are very high, high, moderate, low and safe susceptibility zones, respectively. The best distributions of the LSI of FR and WoE are shown in Figs. 8a and 6b, respectively. The FR and WoE LSI maps show that the spatial distribution are a bit similar, where 65 % of very high and high susceptibility classes are shared between these two models.

4.2.2 Landslide susceptibility assessment using logistic and probit regressions

Approximately 1.2 % of the study area (22 734 training pixel) is used to derive the coefficients of PR and LR. The model-building process for both, the LR and the PR started with 16 prediction factors. The landslide prediction factors considered in this study are shown in Table A1. Nine factors with significance values > 0.05 have been withheld of the analysis in the last step of the process model. While seven factors, which have significance < 0.05; namely hypsometric integral, slope, topographic wetness index, NDVI, precipitation, lithology and aspect, were used (Table 1).

The probit and logistic regression show similarity in the sequence of the factors, where the lithology, the slope aspect and the NDVI are the major factors of landslides occurrences (Fig. 7b).

This means that the factors with an odd more than 1 are positively related to the occurrence of a landslide and the factors less than 1 are negatively related to the landslide occurrence whereas the precipitation and slope factors, which have odd of 1 are neutral to the occurrence of a landslide in the study area. According to Table 1, the odd of slope and precipitation is 1; the hypsometric integral, TWI, clastic and limestone of lithological classes, and N, NE, E, SE and NW aspect directions odds are more than 1; while the rest are less than 1. In particular, the factor "NE aspect" has the strongest effect on the development of landslides than any other parameter, where the odd of the probit and the logistic regressions are 3.95 and 2.33, respectively. The best distribution of the LSI of LR and PR are shown in Figs. 8c and 6d, respectively. The PR and the LR LSI maps show that their spatial distributions are similar, where 99.7 % of very high and high susceptibility classes are shared between these two models

5 Discussion

GIS-based techniques have generally been utilized as requisite tools for landslides susceptibility mapping. In previous studies, FR, LR, and WoE methods were used either separately (e.g. Shahabi et al., 2014; Wang et al., 2013; Pradhan and Lee, 2010; Das et al., 2012), or compared with each other (e.g. Ozdemir and Altural, 2013). In this study, we compared the three above-mentioned models to the PR model, which has never been applied for LSI. Each model has clear advantages and disadvantages. FR and WOE models are simple and easy to apply, while LR and PR models are

NHESSD
3, 1789–1833, 2015

more complex as data need to be converted from GIS to a statistical software program (Park et al., 2013). The FR and WoE methods allow evaluation of relationship between a dependent (landslides) and several independent variables (predicting factors) in only discrete forme. However, the LR and PR allow to evaluate the continuous independent variables in addition to discrete forms (Shahabi et al., 2014; Wang et al., 2013; Schicker and Moon, 2012).

The four LSI maps show that spatial distributions are bit similar. The PR and LR models gave almost the same results. In some areas, the FR and WoE models show significant variations with respect to PR and LR. This is mainly the case in southern and western parts of the study area (Fig. 8). Only 25 % of the very high class is shared among all models.

In order to verify the results of the four LSI models, we made a comparison between them using AUC percentage and R index. According to the results of ROC curve, the final PR, LR and WoE maps yielded somewhat similar AUCs of 81.86, 81.83 and 81.61 %, respectively; while the final FR map yielded an AUC of 78.31 % (Fig. 9a). The PR and LR models ROC curves are almost superimposed (Fig. 9a). In the same vein, the R index for the final WoE map indicates that the sum of very high and high landslides susceptibility classes collected 89.42 % of the validation landslide areas, while the final PR, LR, and FR maps collected 86.29, 86.22, and 84.22 % of the validation landslide areas, respectively (Fig. 9b). All other zones include validation landslide areas < 16 %. The safe susceptibility class of the final WoE map captured 0.75 % of the validation landslide areas less than the final PR, LR, and FR maps where they captured for each of them ~ 1.11 of the validation landslide areas, respectively. However, if we consider both validation results i.e. AUC and R index, WoE can be assumed as the best method used in this paper followed by PR, LR and FR. The differences between the AUC for PR, LR and WoE models are < 0.35 %, while for the R index reach 5 % for very high class, and 3.2 % for very high and high classes. The PR, LR and WoE models are comparatively good estimators for the LSI. Our results indicate that the LR model is better than the FR model and are conform to previous studies (Shahabi et al.,

NHESSD
3, 1789–1833, 2015

2014; Choi et al., 2012; Park et al., 2013; Yilmaz, 2009; Lee et al., 2012). The results of this paper also agree with Suh et al. (2011) which reported that WoE model is better than FR model. Indeed, the AUC of the WoE model is ∼ 3.55 % higher than the AUC of the FR model.

Previous works which applied generalized linear models have only focused on LR. The PR has never been used before for LSI mapping although many popular statistical softwares such as SPSS and R include this function. PR model can give slightly better result than LR model (Bottai et al., 2010). Our results indicate that PR is an applicable approach. the different dataset of factor groups that tested show that the AUCs of the PR model are between 0.02 and 0.25 % higher than the AUC of the LR model (Fig. 9a). The high and very high classes of the *R* index are also very slightly higher for the PR model than for the LR model (Fig. 9b).

In addition to the LSI methods, choosing the predicting factors plays a dominant role to increase the AUC accuracy of LSI map (Carrara et al., 1995; Capitani et al., 2013a; Van Den Eeckhaut et al., 2006). Careful consideration of all relevant factors is required to adequately assess the weightings of factors according to specific site conditions, especially for FR and WoE. It should be noted that number and boundary of classes could highly change the result of the FR and WoE methods. The estimation range of all four models (Fig. 7) indicates that lithology and slope aspects played major roles in frequent landslide occurrences in Mawat area. All models show that lithology is more effective than other factors due to variance in the cohesion and permeability of the rock types (Ozdemir and Altural, 2013; Garcia-Rodriguez et al., 2008; Dai et al., 2001). In addition, the slope aspect have a significant impact for landsliding because it controls the exposure to sunlight, winds, rainfall (Yalcin et al., 2011), and vegetation cover (Garcia-Rodriguez et al., 2008).

The use of HI as prediction factor instead of the curvature increased the AUC accuracy of LSI maps by ∼ 2 %. This significant increase is related to the possibility to compute the HI using a larger kernel size. Thus it can reflects slope shape of major, medium and small landslides. By contrast, curvature is only computed for a 3 by

NHESSD
3, 1789–1833, 2015

3 kernel. This is useful for small landslides but may not be adapted to medium and large landslides. The HI coefficients show that the high convex slope and low concave slopes are more affected by landsliding than other types of slope features. The increase in landslides frequency is also related to the decrease of NDVI value i.e. a lack of appropriate vegetation cover. The landslides frequency is decreasing with increasing precipitation due to a N-NW gradient of $\sim 131\,\mathrm{mm\,yr^{-1}}$. It is known that the role of precipitation as the factor of landslides is strongly affected by the morphological dynamics and geology (Yalcin et al., 2011). Therefore, It seems that the influence of other factors such as lithology and morphological dynamics such as slope aspect and HI is greater compared to the variation of the precipitation.

Combining the TPI with the other significant prediction factors also increased the AUC accuracy of FR and WoE by $\sim 1\,\%$. Density of lineaments (created with TecLines, Rahnama and Gloaguen, 2014a, b) contributed to improve the AUC accuracy of the WoE and FR methods by $\sim 2\,\%$. The TPI and distance to lineaments maps do not have any significant effect to improve LR and PR maps. However, Rahnama et al. (2015) reported that the distance to lineaments map created by TecLines has significant improvement on landslide occurrences in the northeast of Afghanistan not only in FR and WoE but in LR methods as well.

6 Conclusions

For the first time PR was applied together with FR, WoE and LR to compute landslides susceptibility map for the Mawat area, Kurdistan Region, NE Iraq. These four methods have not been compared in terms of accuracy for the landslides susceptibility index mapping before. For this purpose, we utilized 16 prediction factors; most of them were derived from VNIR ASTER satellite data. Two of them (i.e. lithology and slope aspect) have more influence than other factors in landslides occurrences. This study also uses new geomorphic indices as prediction factors in order to increase the estimation accuracy of the LSI. This paper demonstrates that hypsometric integral gives better result

NHESSD
3, 1789–1833, 2015

than slope curvatures, and increases the area under curve accuracy by ∼ 2 %. The use of the hypsometric integral is useful to major, medium and small landslides, while the curvature is only helpful with small landslides. Including a distance to lineaments map that was generated by Teclines toolbox contributed to increase the area under curve accuracy of FR and WoE landslide susceptibility maps by ∼ 2 %. Finally, this study highlights that the behavior of the PR model is similar to LR model, while WoE and FR models are close to one other. All processing steps of the FR and WoE models are relatively simple and easier compared to the PR and LR, which need a preliminary conversion of the data. The comparison of results of this study indicates that the PR, LR and WoE models are good estimators of the LSI. The WoE model has the highest prediction accuracy for the Mawat area. Our work has led us to conclude that PR model can give better result compared to LR model in the LSI, where both validation types show that the PR model is better than the LR model. The AUC of the PR model is always above the AUC of the LR model with different dataset combinations.

Author contributions. Arsalan Ahmed Othman prepared and processed the data and accomplished the study. He wrote the manuscript. Richard Gloaguen outlined the research, and supported the analysis and discussion. He also supervised the writing of the manuscript at all stages. Louis Andreani and Mehdi Rahnama assisted with the extraction of lineaments and geomorphic indices. All authors checked and revised the manuscript.

Acknowledgements. The research was supported by the Ministry of Higher Education and Scientific Research of Iraq (MoHESR), and by the German Academic Exchange Service (DAAD). We are grateful to the Geological Survey of Iraq for providing the data and supporting the fieldwork.

References

Abrams, M. and Hook, S.: ASTER user handbook (Version 2), Report, California Institute of Technology, Pasadena, USA, 2001. 1795

Agard, P., Omrani, J., Jolivet, L., Whitechurch, H., Vrielynck, B., Spakman, W., Monié, P., Meyer, B., and Wortel, R.: Zagros orogeny: a subduction-dominated process, Geol. Mag., 148, 692–725, doi:10.1017/S001675681100046X, 2011. 1793

Akgun, A.: A comparison of landslide susceptibility maps produced by logistic regression, multi-criteria decision, and likelihood ratio methods: a case study at İzmir, Turkey, Landslides, 9, 93–106, doi:10.1007/s10346-011-0283-7, 2012. 1791

Al-Mehaidi, H. M.: Geological investigation of Mawat-Chuwarta area, northeastern Iraq, Report 609, GEOSURV, Baghdad, Iraq, 1974. 1794, 1805

Al-Rubaiay, A. T. and Al-Dulaimi, T. Y.: Series of land use land cover maps of Iraq scale 1 : 250 000, Sulaimaniya quadrangle sheet NI-38-3 (LULCM 10), Report, GEOSURV, Baghdad, Iraq, 2012. 1798

Alavi, M.: Tectonics of Zagros Oroginic Belt of Iran: new data and interpretations, Tectonophysics, 229, 221–238, 1994. 1793

Alavi, M.: Regional stratigraphy of the Zagros Fold – thrust belt of Iran and its proforeland evolution, Am. J. Sci., 304, 1–20, 2004. 1793

Aldrich, J. and Nelson, F.: Linear Probability, Logit, and Probit Models, SAGE Publications, available at: http://books.google.de/books?id=z0tmctgE1OYC (last access: 17 January 2015), 1984. 1802

Althuwaynee, O. F., Pradhan, B., Park, H.-J., and Lee, J. H.: A novel ensemble bivariate statistical evidential belief function with knowledge-based analytical hierarchy process and multivariate statistical logistic regression for landslide susceptibility mapping, Catena, 114, 21–36, doi:10.1016/j.catena.2013.10.011, 2014. 1791, 1802

Atkinson, P. M. and Massari, R.: Generalised linear modelling of susceptibility to landsliding in the central Apennines, Italy, Comput. Geosci., 24, 373–385, 1998. 1791, 1803

Ayalew, L. and Yamagishi, H.: The application of GIS-based logistic regression for landslide susceptibility mapping in the Kakuda-Yahiko Mountains, Central Japan, Geomorphology, 65, 15–31, doi:10.1016/j.geomorph.2004.06.010, 2005. 1798, 1803

NHESSD

3, 1789–1833, 2015

Landslide susceptibility mapping in Mawat area, Kurdistan Region, NE Iraq

A. A. Othman et al.

Ayalew, L., Yamagishi, H., Marui, H., and Kanno, T.: Landslides in Sado Island of Japan: Part II, GIS-based susceptibility mapping with comparisons of results from two methods and verifications, Eng. Geol., 81, 432–445, doi:10.1016/j.enggeo.2005.08.004, 2005. 1791

Baeza, C. and Corominas, J.: Assessment of shallow landslide susceptibility by means of multivariate statistical techniques, Earth Surf. Proc. Land., 26, 1251–1263, 2001. 1804

Bai, S., Wang, J., Zhang, Z., and Cheng, C.: Combined landslide susceptibility mapping after Wenchuan earthquake at the Zhouqu segment in the Bailongjiang Basin, China, Catena, 99, 18–25, doi:10.1016/j.catena.2012.06.012, 2012. 1803

Beven, K. J. and Kirkby, M. J.: A physically based, variable contributing area model of basin hydrology/Un modelle a base physique de zone d'appel variable de l'hydrologie du bassin versant, Hydrol. Sci. Bull., 24, 43–69, doi:10.1080/02626667909491834, 1979. 1799

Bottai, M., Cai, B., and McKeown, R. E.: Logistic quantile regression for bounded outcomes, Stat. Med., 29, 309–317, 2010. 1810

Buday, T. and Suk, M.: Report on the geological survay in NE Iraq between Halabja and Qala'a Diza, Report, GEOSURV, Baghdad, Iraq, 1978. 1794

Calo, F., Ardizzone, F., Castaldo, R., Lollino, P., Tizzani, P., Guzzetti, F., Lanari, R., Angeli, M.-G., Pontoni, F., and Manunta, M.: Enhanced landslide investigations through advanced DInSAR techniques: the Ivancich case study, Assisi, Italy, Remote Sens. Environ., 142, 69–82, doi:10.1016/j.rse.2013.11.003, 2014. 1790

Capitani, M., Ribolini, A., and Bini, M.: The slope aspect: a predisposing factor for landsliding?, CR Geosci., 345, 427–438, doi:10.1016/j.crte.2013.11.002, 2013a. 1791, 1792, 1798, 1810

Capitani, M., Ribolini, A., and Federici, P. R.: Influence of deep-seated gravitational slope deformations on landslide distributions: a statistical approach, Geomorphology, 201, 127–134, 2013b. 1798

Carrara, A., Cardinali, M., Guzzetti, F., and Reichenbach, P.: GIS technology in mapping landslide hazard, in: Geographical Information Systems in Assessing Natural Hazards, vol. 5 of Advances in Natural and Technological Hazards Research, book section 8, Springer Netherlands, 135–175, doi:10.1007/978-94-015-8404-3_8, 1995. 1791, 1792, 1810

Chen, W., Li, X., Wang, Y., and Liu, S.: Landslide susceptibility mapping using LiDAR and DMC data: a case study in the Three Gorges area, China, Environ. Earth Sci., 70, 673–685, 2013. 1799

Choi, J., Oh, H.-J., Lee, H.-J., Lee, C., and Lee, S.: Combining landslide susceptibility maps obtained from frequency ratio, logistic regression, and artificial neural network models using

ASTER images and GIS, Eng. Geol., 124, 12–23, doi:10.1016/j.enggeo.2011.09.011, 2012. 1796, 1798, 1810

CHRR, CIESIN, and NGI: Global Landslide Hazard Distribution, available at: http://sedac.ciesin.columbia.edu/data/set/ndh-landslide-hazard-distribution (last acces: 17 January 2015), 2005. 1793

Conforti, M., Pascale, S., Robustelli, G., and Sdao, F.: Evaluation of prediction capability of the artificial neural networks for mapping landslide susceptibility in the Turbolo River catchment (northern Calabria, Italy), Catena, 113, 236–250, doi:10.1016/j.catena.2013.08.006, 2014. 1791

Corsini, A., Cervi, F., and Ronchetti, F.: Weight of evidence and artificial neural networks for potential groundwater spring mapping: an application to the Mt. Modino area (Northern Apennines, Italy), Geomorphology, 111, 79–87, doi:10.1016/j.geomorph.2008.03.015, 2009. 1801

Dai, F. C., Lee, C. F., Li, J., and Xu, Z. W.: Assessment of landslide susceptibility on the natural terrain of Lantau Island, Hong Kong, Environ. Geol., 40, 381–391, doi:10.1007/s002540000163, 2001. 1810

Das, I., Stein, A., Kerle, N., and Dadhwal, V. K.: Landslide susceptibility mapping along road corridors in the Indian Himalayas using Bayesian logistic regression models, Geomorphology, 179, 116–125, doi:10.1016/j.geomorph.2012.08.004, 2012. 1808

De Reu, J., Bourgeois, J., Bats, M., Zwertvaegher, A., Gelorini, V., De Smedt, P., Chu, W., Antrop, M., De Maeyer, P., Finke, P., Van Meirvenne, M., Verniers, J., and Crombe, P.: Application of the topographic position index to heterogeneous landscapes, Geomorphology, 186, 39–49, 2013. 1798

DigitalGlobe: QuickBird Imagery Products – Product Guid, Report, Global Land Cover Facility, Longmont, Colorado, USA, 2006. 1795

Ercanoglu, M.: Landslide susceptibility assessment of SE Bartin (West Black Sea region, Turkey) by artificial neural networks, Nat. Hazards Earth Syst. Sci., 5, 979–992, doi:10.5194/nhess-5-979-2005, 2005. 1791

Erener, A. and Duzgun, H. S. B.: Landslide susceptibility assessment: what are the effects of mapping unit and mapping method?, Environ. Earth Sci., 66, 859–877, 2012. 1803

ESRI: ArcGIS Desktop: Release 10, USA, 2011. 1796

ESRI: ArcGIS help library, Report, Environmental Systems Research Institute, USA, 2012. 1797

Fawcett, T.: An introduction to ROC analysis, Pattern Recogn. Lett., 27, 861–874, doi:10.1016/j.patrec.2005.10.010, 2006. 1804
Fouad, S. F.: Tectonic map of Iraq, scale 1 : 1,000,000, GEOSURV, Baghdad, Iraq, 2010. 1793, 1825
García-Rodríguez, M. J. and Malpica, J. A.: Assessment of earthquake-triggered landslide susceptibility in El Salvador based on an Artificial Neural Network model, Nat. Hazards Earth Syst. Sci., 10, 1307–1315, doi:10.5194/nhess-10-1307-2010, 2010. 1791
Garcia-Rodriguez, M. J., Malpica, J. A., Benito, B., and Diaz, M.: Susceptibility assessment of earthquake-triggered landslides in El Salvador using logistic regression, Geomorphology, 95, 172–191, 2008. 1797, 1810
Guzzetti, F.: Landslide hazard and risk assessment, dissertation, Bonn University, Bonn, 2006. 1791
Guzzetti, F., Carrara, A., Cardinali, M., and Reichenbach, P.: Landslide hazard evaluation: a review of current techniques and their application in a multi-scale study, Central Italy, Geomorphology, 31, 181–216, doi:10.1016/S0169-555X(99)00078-1, 1999. 1791, 1801
Guzzetti, F., Cardinali, M., Reichenbach, P., and Carrara, A.: Comparing landslide maps: a case study in the Upper Tiber River Basin, Central Italy, Environ. Manage., 25, 247–263, doi:10.1007/s002679910020, 2000. 1790
Guzzetti, F., Reichenbach, P., Cardinali, M., Galli, M., and Ardizzone, F.: Probabilistic landslide hazard assessment at the basin scale, Geomorphology, 72, 272–299, 2005. 1791
Intarawichian, N. and Dasananda, S.: Frequency ratio model based landslide susceptibility mapping in lower Mae Chaem watershed, Northern Thailand, Environ. Earth Sci., 64, 2271–2285, doi:10.1007/s12665-011-1055-3, 2011. 1804
Jassim, S. Z. and Goff, J. C.: Geology of Iraq, Dolin, Brno, Czech Republic, 2006. 1793, 1794, 1825
Kayastha, P., Dhital, M. R., and De Smedt, F.: Application of the analytical hierarchy process (AHP) for landslide susceptibility mapping: a case study from the Tinau watershed, west Nepal, Comput. Geosci., 52, 398–408, doi:10.1016/j.cageo.2012.11.003, 2013. 1792
Kleinbaum, D. and Klein, M.: Survival Analysis: a Self-Learning Text, 3rd Edn., Springer, available at: http://books.google.de/books?id=v3FZngEACAAJ (last access: 13 January 2015), 2011. 1802
Lawa, F. A., Koyi, H., and Ibrahim, A.: Tectono-stratigraphic evolution of the NW segment of the Zagros fold-thrust belt, Kurdistan, NE Iraq, J. Petrol. Geol., 36, 75–96, 2013. 1793

NHESSD
3, 1789–1833, 2015

Landslide susceptibility mapping in Mawat area, Kurdistan Region, NE Iraq

A. A. Othman et al.

Lee, M. J., Choi, J. W., Oh, H. J., Won, J. S., Park, I., and Lee, S.: Ensemble-based landslide susceptibility maps in Jinbu area, Korea, Environ. Earth Sci., 67, 23–37, a 2012. 1810

Lee, S.: Landslide detection and susceptibility mapping in the Sagimakri area, Korea using KOMPSAT-1 and weight of evidence technique, Environ. Earth Sci., 70, 3197–3215, 2013. 1791

Lee, S. and Min, K.: Statistical analysis of landslide susceptibility at Yongin, Korea, Environ. Geol., 40, 1095–1113, doi:10.1007/s002540100310, 2001. 1791, 1797

Lee, S. and Talib, J. A.: Probabilistic landslide susceptibility and factor effect analysis, Environ. Geol., 47, 982–990, 2005. 1791, 1792, 1800

Lee, S., Ryu, J., Min, K., and Won, J.: Development of two artificial neural network methods for landslide susceptibility analysis, in: Geoscience and Remote Sensing Symposium, 2001, IGARSS '01, IEEE 2001 International, vol. 5, 9–13 July 2001, Sydney, NSW, 2364–2366, 2001. 1791

Lee, S., Choi, J., Chwae, U., and Chang, B.: Landslide susceptibility analysis using weight of evidence, vol. 5, 2865–2867, available at: http://www.scopus.com/inward/record.url?eid=2-s2.0-0036398928&partnerID=40&md5=dae165d8fbccd72155aae1371bfe966d (last access: 13 January 2015), 2002a. 1791

Lee, S., Choi, J., and Min, K.: Landslide susceptibility analysis and verification using the Bayesian probability model, Environ. Geol., 43, 120–131, doi:10.1007/s00254-002-0616-x, 2002b. 1800

Lepore, C., Kamal, S. A., Shanahan, P., and Bras, R. L.: Rainfall-induced landslide susceptibility zonation of Puerto Rico, Environ. Earth Sci., 66, 1667–1681, 2012. 1800

Lin, L. L., Wang, C. W., Chiu, C. L., and Ko, Y. C.: A study of rationality of slopeland use in view of land preservation, Paddy Water Environ., 9, 257–266, 2011. 1797

Ma'ala, K.: The geology of Sulaimaniya Quadrangle sheet no. NI-38-3, Scale 1 : 25 0000, Report, GEOSURV, Baghdad, Iraq, 2008. 1794

Mancini, F., Ceppi, C., and Ritrovato, G.: GIS and statistical analysis for landslide susceptibility mapping in the Daunia area, Italy, Nat. Hazards Earth Syst. Sci., 10, 1851–1864, doi:10.5194/nhess-10-1851-2010, 2010. 1797

Mantovani, F., Soeters, R., and Van Westen, C. J.: Remote sensing techniques for landslide studies and hazard zonation in Europe, Geomorphology, 15, 213–225, doi:10.1016/0169-555X(95)00071-C, 1996. 1791

McCullagh, P. and Nelder, J.: Generalized Linear Models, Routledge, Chapman & Hall, Incorporated, available at: http://books.google.de/books?id=_ku8QgAACAAJ (last access: 13 January 2015), 1983. 1802

Metternicht, G., Hurni, L., and Gogu, R.: Remote sensing of landslides: an analysis of the potential contribution to geo-spatial systems for hazard assessment in mountainous environments, Remote Sens. Environ., 98, 284–303, doi:10.1016/j.rse.2005.08.004, 2005. 1791

Meyer, N. K., Schwanghart, W., Korup, O., Romstad, B. A., and Etzelmüller, B.: Estimating the topographic predictability of debris flows, Geomorphology, 207, 114–125, doi:10.1016/j.geomorph.2013.10.030, 2014. 1800, 1801

Mohammady, M., Pourghasemi, H. R., and Pradhan, B.: Landslide susceptibility mapping at Golestan Province, Iran: a comparison between frequency ratio, Dempster-Shafer, and weights-of-evidence models, J. Asian Earth Sci., 61, 221–236, doi:10.1016/j.jseaes.2012.10.005,2012. 1800, 1801

Moore, I. D., Grayson, R. B., and Ladson, A. R.: Digital terrain modelling: a review of hydrological, geomorphological, and biological applications, Hydrol. Process., 5, 3–30, 1991. 1797

Mărgărint, M. C., Grozavu, A., and Patriche, C. V.: Assessing the spatial variability of coefficients of landslide predictors in different regions of Romania using logistic regression, Nat. Hazards Earth Syst. Sci., 13, 3339–3355, doi:10.5194/nhess-13-3339-2013, 2013. 1804

Nefeslioglu, H. A., Duman, T. Y., and Durmaz, S.: Landslide susceptibility mapping for a part of tectonic Kelkit Valley (Eastern Black Sea region of Turkey), Geomorphology, 94, 401–418, 2008a. 1796

Nefeslioglu, H. A., Gokceoglu, C., and Sonmez, H.: An assessment on the use of logistic regression and artificial neural networks with different sampling strategies for the preparation of landslide susceptibility maps, Eng. Geol., 97, 171–191, 2008b. 1797

Othman, A. and Gloaguen, R.: Automatic extraction and size distribution of landslides in Kurdistan Region, NE Iraq, Remote Sensing, 5, 2389–2410, doi:10.3390/rs5052389, 2013a. 1791, 1793, 1794, 1795, 1799, 1803

Othman, A. and Gloaguen, R.: River courses affected by landslides and implications for hazard assessment: a high resolution remote sensing case study in NE Iraq–W Iran, Remote Sensing, 5, 1024–1044, doi:10.3390/rs5031024 2013b. 1793, 1797, 1799

Othman, A. and Gloaguen, R.: Improving lithological mapping by SVM classification of spectral and morphological features: the discovery of a new chromite body in the Mawat Ophiolite Complex (Kurdistan, NE Iraq), Remote Sensing, 6, 6867–6896, doi:10.3390/rs6086867, 2014 1798, 1805

Ozdemir, A. and Altural, T.: A comparative study of frequency ratio, weights of evidence and logistic regression methods for landslide susceptibility mapping: Sultan Mountains, SW Turkey, J. Asian Earth Sci., 64, 180–197, doi:10.1016/j.jseaes.2012.12.014, 2013. 1791, 1792, 1796, 1800, 1801, 1803, 1804, 1808, 1810

Park, S., Choi, C., Kim, B., and Kim, J.: Landslide susceptibility mapping using frequency ratio, analytic hierarchy process, logistic regression, and artificial neural network methods at the Inje area, Korea, Environ. Earth Sci., 68, 1443–1464, doi:10.1007/s12665-012-1842-5, 2013. 1800, 1809, 1810

Peng, L., Niu, R., Huang, B., Wu, X., Zhao, Y., and Ye, R.: Landslide susceptibility mapping based on rough set theory and support vector machines: a case of the Three Gorges area, China, Geomorphology, 204, 287–301, doi:10.1016/j.geomorph.2013.08.013, 2014. 1791

Perez-Pena, J., Azanon, J., and Azor, A.: CalHypso: an ArcGIS extension to calculate hypsometric curves and their statistical moments. Applications to drainage basin analysis in {SE} Spain, Comput. Geosci., 35, 1214–1223, doi:10.1016/j.cageo.2008.06.006, 2009. 1797

Petley, D.: Global patterns of loss of life from landslides, Geology, 40, 927–930, 2012. 1790

Pike, R. J. and Wilson, S. E.: Elevation-relief ratio, hypsometric integral, and geomorphic area-altitude analysis, Bull. Geol. Soc. Am., 82, 1079–1084, 1971. 1797

Poli, S. and Sterlacchini, S.: Landslide representation strategies in susceptibility studies using weights-of-evidence modeling technique, Nat. Resour. Res., 16, 121–134, 2007. 1804

Pradhan, B. and Lee, S.: Landslide susceptibility assessment and factor effect analysis: backpropagation artificial neural networks and their comparison with frequency ratio and bivariate logistic regression modelling, Environ. Model. Softw., 25, 747–759, doi:10.1016/j.envsoft.2009.10.016, 2010. 1808

Pradhan, B., Singh, R. P., and Buchroithner, M. F.: Estimation of stress and its use in evaluation of landslide prone regions using remote sensing data, Adv. Space Res., 37, 698–709, 2006. 1798

Qiao, G., Lu, P., Scaioni, M., Xu, S., Tong, X., Feng, T., Wu, H., Chen, W., Tian, Y., Wang, W., and Li, R.: Landslide investigation with remote sensing and sensor network: from susceptibility mapping and scaled-down simulation towards in situ sensor network design, Remote Sensing, 5, 4319–4346, 2013. 1791

NHESSD

3, 1789–1833, 2015

Landslide susceptibility mapping in Mawat area, Kurdistan Region, NE Iraq

A. A. Othman et al.

Title Page
Abstract | Introduction
Conclusions | References
Tables | Figures
◂◂ | ▸▸
◂ | ▸
Back | Close
Full Screen / Esc
Printer-friendly Version
Interactive Discussion

Rahnama, M. and Gloaguen, R.: TecLines: a MATLAB-based toolbox for tectonic lineament analysis from satellite images and DEMs, Part 2: Line segments linking and merging, Remote Sensing, 6, 11468–11493, doi:10.3390/rs61111468, 2014a. 1795, 1811

Rahnama, M. and Gloaguen, R.: TecLines: a MATLAB-based toolbox for tectonic lineament analysis from satellite images and DEMs, Part 1: Line segment detection and extraction, Remote Sensing, 6, 5938–5958, doi:10.3390/rs6075938, 2014b. 1795, 1798, 1811

Rahnama, M., Gloaguen, R., and Othman, A.: The Effect of Lineaments on the Accuracy of Landslide Susceptibility Mapping: a Case Study in Part of Badakhshan Province, Afghanistan, TU Freiberg, Freiberg, Germany, 2015. 1811

Regmi, N. R., Giardino, J. R., and Vitek, J. D.: Assessing susceptibility to landslides: using models to understand observed changes in slopes, Geomorphology, 122, 25–38, 2010. 1800

Rouse, J., Haas, R., Schelle, J., Deering, D., and Harlan, J.: Monitoring the vernal advancement or retrogradation of natural vegetation, Report, NASA, College Station, Texas, 1974. 1799

Santacana, N. A., Baeza, B., Corominas, J., De Paz, A., and Marturiá, J.: A GIS-based multivariate statistical analysis for shallow landslide susceptibility mapping in La Pobla de Lillet Area (Eastern Pyrenees, Spain), Nat. Hazards, 30, 281–295, doi:10.1023/B:NHAZ.0000007169.28860.80, 2003. 1804

Scaioni, M., Longoni, L., Melillo, V., and Papini, M.: Remote sensing for landslide investigations an overview of recent achievements and perspectives, Remote Sensing, 6, 9600–9652, doi:10.3390/rs6109600, 2014. 1791

Schicker, R. and Moon, V.: Comparison of bivariate and multivariate statistical approaches in landslide susceptibility mapping at a regional scale, Geomorphology, 161–162, 40–57, doi:10.1016/j.geomorph.2012.03.036, 2012. 1796, 1804, 1809

Shahabi, H., Khezri, S., Ahmad, B. B., and Hashim, M.: Landslide susceptibility mapping at central Zab basin, Iran: a comparison between analytical hierarchy process, frequency ratio and logistic regression models, Catena, 115, 55–70, doi:10.1016/j.catena.2013.11.014, 2014. 1791, 1799, 1800, 1804, 1808, 1809

Shahzad, F. and Gloaguen, R.: TecDEM: a MATLAB based toolbox for tectonic geomorphology, Part 2: Surface dynamics and basin analysis, Comput. Geosci., 37, 261–271, doi:10.1016/j.cageo.2010.06.009, 2011. 1795

Sissakian, V. K.: Geological evolution of the Iraqi Mesopotamia Foredeep, inner platform and near surroundings of the Arabian Plate, J. Asian Earth Sci., 31, 152–163, doi:10.1016/j.jseaes.2012.09.032, 2012. 1825

Sissakian, V. K., Ahad, I. A., and Qambar, A.: Series of geological hazards map of Iraq sulimanyah quadrangle, scale 1 : 250 000, sheet No. NI-38-3, Report, GEOSURV, Baghdad, Iraq, 2004. 1794

Smirnov, V. and Nelidov, V.: Report on 1 : 200,000 prospecting-correlation of the Sulimaniya-Choarta-Penjwin area carried out in 1961, Report, GEOSURV, Baghdad, Iraq, 1962. 1794

Strahler, A. N.: Hypsometric (area-altitude) analysis of erosional topography, Geol. Soc. Am. Bull., 63, 1117–1142, 1952. 1797

Suh, J., Choi, Y., Roh, T.-D., Lee, H.-J., and Park, H.-D.: National-scale assessment of landslide susceptibility to rank the vulnerability to failure of rock-cut slopes along expressways in Korea, Environ. Earth Sci., 63, 619–632, doi:10.1007/s12665-010-0729-6, 2011. 1810

Thiery, Y., Malet, J. P., Sterlacchini, S., Puissant, A., and Maquaire, O.: Landslide susceptibility assessment by bivariate methods at large scales: application to a complex mountainous environment, Geomorphology, 92, 38–59, 2007. 1803

Tseng, C. M., Lin, C. W., and Hsieh, W. D.: Landslide susceptibility analysis by means of event-based multi-temporal landslide inventories, Nat. Hazards Earth Syst. Sci. Discuss., 3, 1137–1173, doi:10.5194/nhessd-3-1137-2015, 2015. 1791

Van Den Eeckhaut, M., Vanwalleghem, T., Poesen, J., Govers, G., Verstraeten, G., and Vandekerckhove, L.: Prediction of landslide susceptibility using rare events logistic regression: a case-study in the Flemish Ardennes (Belgium), Geomorphology, 76, 392–410, doi:10.1016/j.geomorph.2005.12.003, 2006. 1791, 1792, 1803, 1810

Van Den Eeckhaut, M., Moeyersons, J., Nyssen, J., Abraha, A., Poesen, J., Haile, M., and Deckers, J.: Spatial patterns of old, deep-seated landslides: a case-study in the northern Ethiopian highlands, Geomorphology, 105, 239–252, doi:10.1016/j.geomorph.2008.09.027, 2009. 1800

Wang, L.-J., Sawada, K., and Moriguchi, S.: Landslide susceptibility analysis with logistic regression model based on FCM sampling strategy, Comput. Geosci., 57, 81–92, doi:10.1016/j.cageo.2013.04.006, 2013. 1792, 1797, 1800, 1808, 1809

Weiss, A.: Topographic position and landforms analysis, ESRI users conference, San Diego, CA, 2001. 1798

Xu, C., Xu, X., Dai, F., and Saraf, A. K.: Comparison of different models for susceptibility mapping of earthquake triggered landslides related with the 2008 Wenchuan earthquake in China, Comput. Geosci., 46, 317–329, doi:10.1016/j.cageo.2012.01.002, 2012. 1797, 1803

Yalcin, A., Reis, S., Aydinoglu, A. C., and Yomralioglu, T.: A GIS-based comparative study of frequency ratio, analytical hierarchy process, bivariate statistics and logistics regression methods for landslide susceptibility mapping in Trabzon, NE Turkey, Catena, 85, 274–287, doi:10.1016/j.catena.2011.01.014, 2011. 1797, 1810, 1811

Yao, X., Tham, L. G., and Dai, F. C.: Landslide susceptibility mapping based on Support Vector Machine: a case study on natural slopes of Hong Kong, China, Geomorphology, 101, 572–582, doi:10.1016/j.geomorph.2008.02.011, 2008. 1791

Yesilnacar, E. and Topal, T.: Landslide susceptibility mapping: a comparison of logistic regression and neural networks methods in a medium scale study, Hendek region (Turkey), Eng. Geol., 79, 251–266, doi:10.1016/j.enggeo.2005.02.002, 2005. 1803

Yilmaz, I.: Landslide susceptibility mapping using frequency ratio, logistic regression, artificial neural networks and their comparison: a case study from Kat landslides (Tokat-Turkey), Comput. Geosci., 35, 1125–1138, doi:10.1016/j.cageo.2008.08.007, 2009. 1810

Zêzere, J. L.: Landslide susceptibility assessment considering landslide typology. A case study in the area north of Lisbon (Portugal), Nat. Hazards Earth Syst. Sci., 2, 73–82, doi:10.5194/nhess-2-73-2002, 2002. 1791

Zhao, C., Lu, Z., Zhang, Q., and de la Fuente, J.: Large-area landslide detection and monitoring with ALOS/PALSAR imagery data over Northern California and Southern Oregon, USA, Remote Sens. Environ., 124, 348–359, doi:10.1016/j.rse.2012.05.025, 2012. 1791

NHESSD

3, 1789–1833, 2015

Landslide susceptibility mapping in Mawat area, Kurdistan Region, NE Iraq

A. A. Othman et al.

Table 1. Results obtained for the probit and logistic regressions models.

Coefficient (X)	(β) Probit estimation	(β) Logistic estimation	Odd ratio of probit	Odd ratio of logistic
(Intercept)	−2.526	−4.233		
HI	0.6125	1.029	1.84	2.8
Slope (°)	0.0012	0.0015	1	1
TWI	0.0229	0.0384	1.02	1.04
NDVI	−3.4	−5.613	0.03	0
Precipitation (mm)	0.0028	0.0047	1	1
Lithology				
Clastic	0.210	0.317	1.28	1.47
Conglomerate	−2.939	−5.894	0.06	0
Gabbro to diorite	−0.767	−1.324	0.48	0.28
Gabbro	−0.769	−1.318	0.49	0.3
Limestone, marble	0.001	−0.006	1.03	1.05
Metabasalt and basalt	−0.341	−0.568	0.73	0.59
Ultramafic	−0.669	−1.107	0.51	0.33
Water	−2.916	−5.864	0.06	0
Flood plain and valley fill	−2.924	−5.873	0.06	0
Aspect (degree from north)				
Flat	−2.117	−4.898	0.07	0
337.5–22.5	0.629	1.014	1.88	2.76
22.5–67.5	0.845	1.374	2.33	3.95
67.5–112.5	0.682	1.102	1.98	3.01
112.5–157.5	0.169	0.271	1.18	1.31
157.5–202.5	−0.316	−0.549	0.73	0.58
202.5–247.5	−0.138	−0.23	0.87	0.79
247.5–292.5	−0.313	−0.546	0.74	0.57
292.5–337.5	0.672	1.093	1.96	2.98

NHESSD
3, 1789–1833, 2015

Table A1. Results obtained for the weights of evidence and frequency ratio models.

Factor	Class	FR		WOE	
		FR	W+	W−	C
1 – Precipitation (mm)	> 833	1.82	0.599	−0.312	0.911
	833–862	1.186	0.170	−0.036	0.206
	862–882	0.781	−0.247	0.068	−0.315
	> 882	0.448	−0.804	0.298	−1.102
2 – Lithology	Clastic (sandstone, siltstone and claystone)	1.799	0.587	−0.030	0.617
	Conglomerate	0.010	−4.571	0.020	−4.590
	Gabbro to diorite with ultramafic inclusions	2.195	0.786	−0.009	0.795
	Gabbro	0.168	−1.785	0.137	−1.922
	Limestone, marble, calc schist and clsstics	1.227	0.204	−0.132	0.336
	Metabasalt and basalt	1.113	0.107	−0.050	0.158
	Ultramafic	1.042	0.41	−0.004	0.045
	Water	0	0	−0.001	0.001
	Flood plain and valley fill sediments	0	0	0.012	−0.012
3 – Land cover	Urban and Built-up Land	0	0.000	0.001	−0.001
	Vegetated Land	0.576	−0.552	0.091	−0.644
	Cultivated Land	0	0.000	0.000	0.000
	Burn Land	0.445	0.000	0.000	0.000
	Harvested Land	1.353	0.302	−0.038	0.340
	Igneous and/or Metamorphic Rocks	0.934	−0.069	0.052	−0.121
	Sedimentary Rocks	1.279	0.246	−0.110	0.356
4 – Elevation (m)	663–900	1.154	0.143	−0.019	0.162
	901–1100	1.442	0.366	−0.112	0.478
	1101–1300	0.856	−0.155	0.037	−0.192
	1301–1500	0.259	−1.350	0.156	−1.507
	1501–1700	0.882	−0.125	0.023	−0.148
	1701–1900	2.118	0.750	−0.118	0.869
	1901–2100	0.527	−0.641	0.020	−0.660
	2101–2360	1.206	0.187	−0.002	0.190
5 – Slope (°)	< 5	0.310	−1.171	0.041	−1.212
	5–10	0.663	−0.411	0.048	−0.459
	10–15	1.191	0.175	−0.040	0.215
	15–20	1.399	0.336	−0.090	0.426
	20–25	1.135	0.127	−0.027	0.154
	25–30	0.904	−0.101	0.014	−0.116
	30–35	0.716	−0.334	0.027	−0.361
	> 35	0.933	−0.069	0.006	−0.075
6 – Distance to lineaments (m)	< 100	1.165	0.15	−0.021	0.173
	100–200	1.052	0.051	−0.007	0.058
	200–300	1.078	0.075	−0.012	0.087
	300–400	0.893	−0.113	0.016	−0.129
	400–500	0.867	−0.142	0.018	−0.160
	500–750	1.039	0.038	−0.010	0.048
	750–1000	1.287	0.252	−0.033	0.285
	1000–1500	0.585	−0.536	0.026	−0.562
	> 1500	0.203	−1.596	0.015	−1.611
7 – Distance to drainage (m)	< 100	0.965	−0.036	0.023	−0.059
	100–200	0.961	−0.040	0.015	−0.055
	200–300	1.035	0.034	−0.008	0.042
	300–400	1.322	0.280	−0.035	0.314
	400–500	0.855	−0.156	0.006	−0.162
	> 500	0.499	−0.695	0.007	−0.702

Factor	Class	FR		WOE	
		FR	W+	W−	C
8-Drainage density (m km^{-2})	< 1.25	0.892	−0.114	0.009	−0.123
	1.25–1.55	1.534	0.428	−0.094	0.522
	1.55–1.85	1.107	0.101	−0.040	0.141
	1.85–2.15	0.713	−0.338	0.144	−0.483
	> 2.15	1.024	0.024	−0.005	0.029
9 – Aspect (degree from north)	Flat	0	0.000	0.001	−0.001
	337.5–−22.5	1.200	0.182	−0.028	0.210
	22.5–−67.5	2.079	0.732	−0.162	0.894
	67.5–−112.5	2.043	0.715	−0.150	0.865
	112.5–−157.5	0.700	−0.356	0.038	−0.394
	157.5–−202.5	0.211	−1.554	0.105	−1.659
	202.5–−247.5	0.324	−1.127	0.098	−1.225
	247.5–−292.5	0.523	−0.649	0.074	−0.723
	292.5–−337.5	1.069	0.067	−0.010	0.077
10 – Curvature (1/m)	< (−3)	0.878	−0.413	0.015	−0.428
	(−3)–(−1)	1.012	−0.129	0.020	−0.148
	(−1)–0	1.044	−0.050	0.016	−0.066
	0–1	1.028	−0.055	0.034	−0.090
	> 1	0.898	−0.347	0.061	−0.408
11 – Plan curvature (1/m)	< (−1)	1.01	−0.348	0.030	−0.378
	(−1)–(−0.5)	1.057	−0.120	0.016	−0.136
	(−0.5)–0	1.046	0.001	0.000	0.001
	0–0.5	1.004	−0.043	0.019	−0.062
	0.5–1	0.899	−0.238	0.029	−0.267
	> 1	0.922	−0.437	0.039	−0.476
12 – Profile curvature (1/m)	< (−1)	0.865	−0.512	0.044	−0.556
	(−1)–(−0.5)	0.995	−0.184	0.021	−0.205
	(−0.5)–0	1.055	−0.035	0.011	−0.046
	0–0.5	1.02	−0.034	0.015	−0.049
	0.5–1	1.023	−0.093	0.012	−0.105
	> 1	0.928	−0.284	0.030	−0.315
13 – Hypsometric integral	< 0.2	0.144	−1.937	0.047	−1.985
	0.2–0.35	0.838	−0.177	0.024	−0.201
	0.35–0.425	1.705	0.533	−0.235	0.769
	0.425–0.5	0.952	−0.049	0.025	−0.074
	0.5–0.6	0.638	−0.450	0.100	−0.551
	> 0.6	1.168	0.155	−0.003	0.158
14 – TWI	< 6	0.828	−0.188	0.057	−0.245
	6–7	0.919	−0.084	0.013	−0.098
	7–8	1.040	0.039	−0.010	0.050
	8–9	1.091	0.087	−0.020	0.107
	9–10	1.064	0.062	−0.008	0.070
	> 10	1.205	0.187	−0.028	0.214
15– TPI	< −65	1.123	0.116	−0.036	0.152
	−65–0	1.085	0.082	−0.042	0.124
	0–100	1.088	0.084	−0.042	0.127
	> 100	0.368	−1.000	0.092	−1.092
16 – NDVI	< 0.12	1.105	0.099	−0.026	0.126
	0.12–0.15	1.268	0.238	−0.096	0.333
	0.15–0.18	1.190	0.174	−0.053	0.228
	0.18–0.22	0.730	−0.315	0.052	−0.367
	> 0.22	0.489	−0.715	0.098	−0.813

NHESSD
3, 1789–1833, 2015

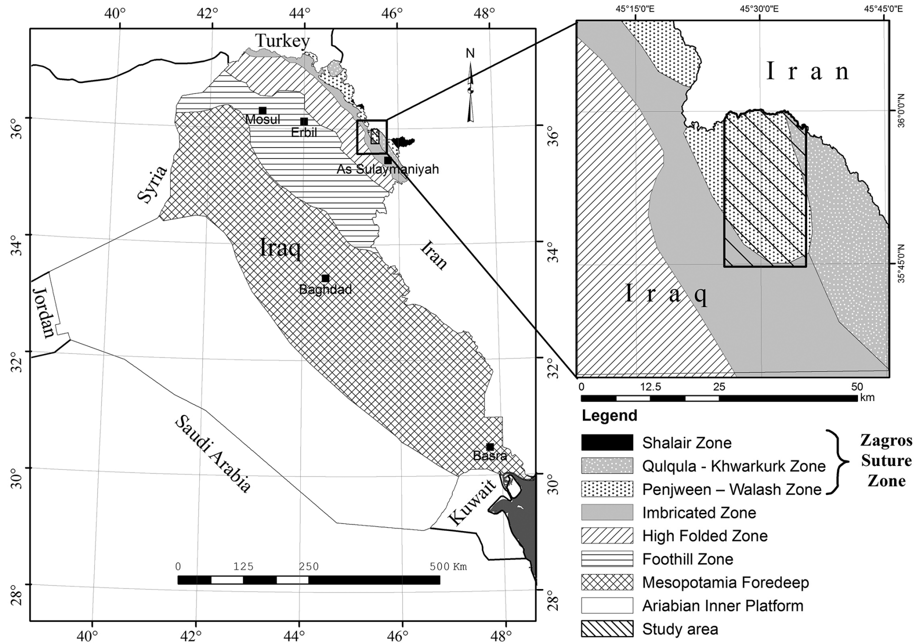

Figure 1. Tectonic map showing the location of the study area which comprises of the Imbricated Zone (IZ) and the Zagros Suture Zone (ZSZ) (Fouad, 2010; Jassim and Goff, 2006; Sissakian, 2012).

NHESSD
3, 1789–1833, 2015

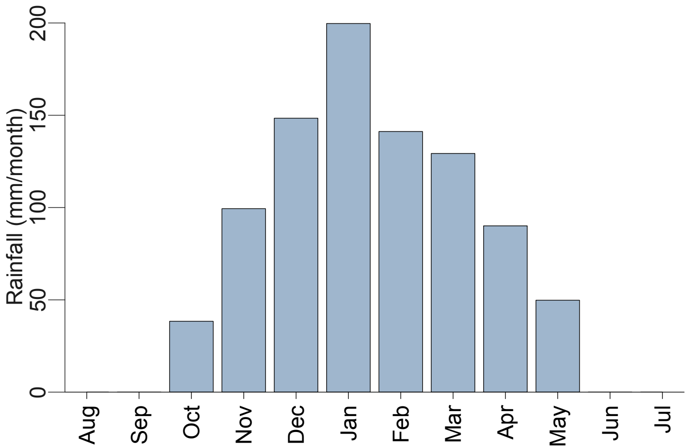

Figure 2. Monthly precipitation in the study area based on data from 2000 to 2006 (the Agro-Meteorological Department of the General Directorate of Research and Agricultural Extension of the Ministry of Agriculture of the Kurdistan Regional Government).

NHESSD
3, 1789–1833, 2015

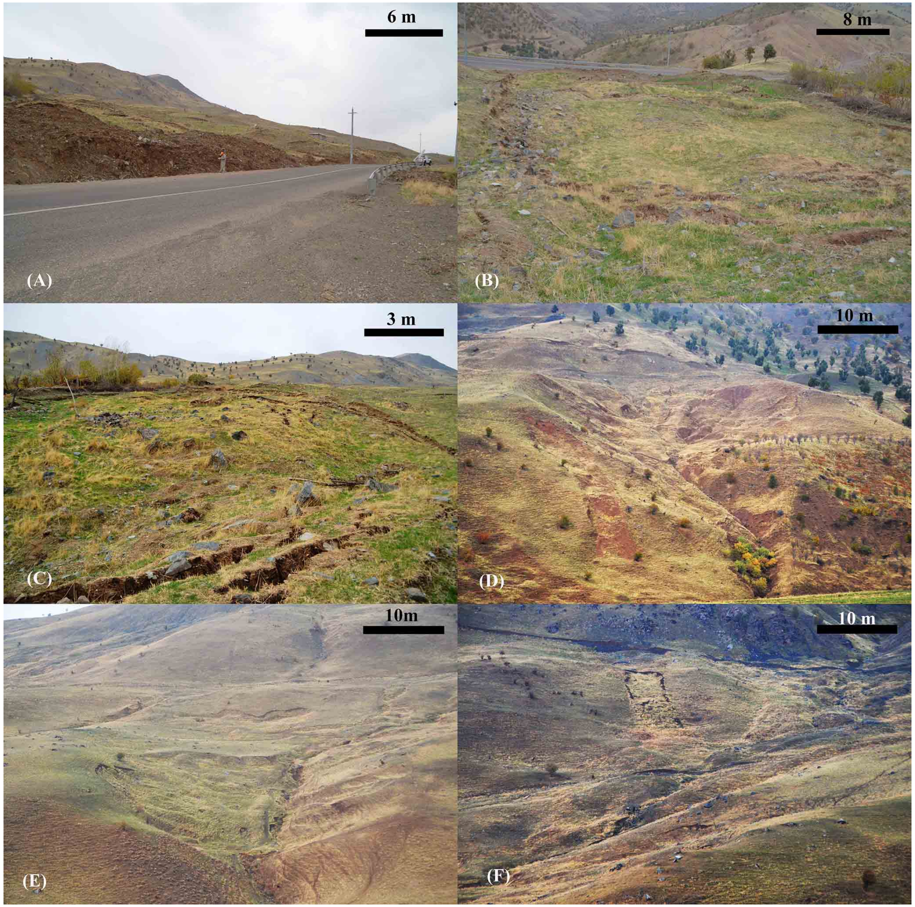

Figure 3. Typical examples of landslides within the study area, where **(a–c)** slump in south of Kanaro village; **(d–f)** rock slide in the study area south of Basne village.

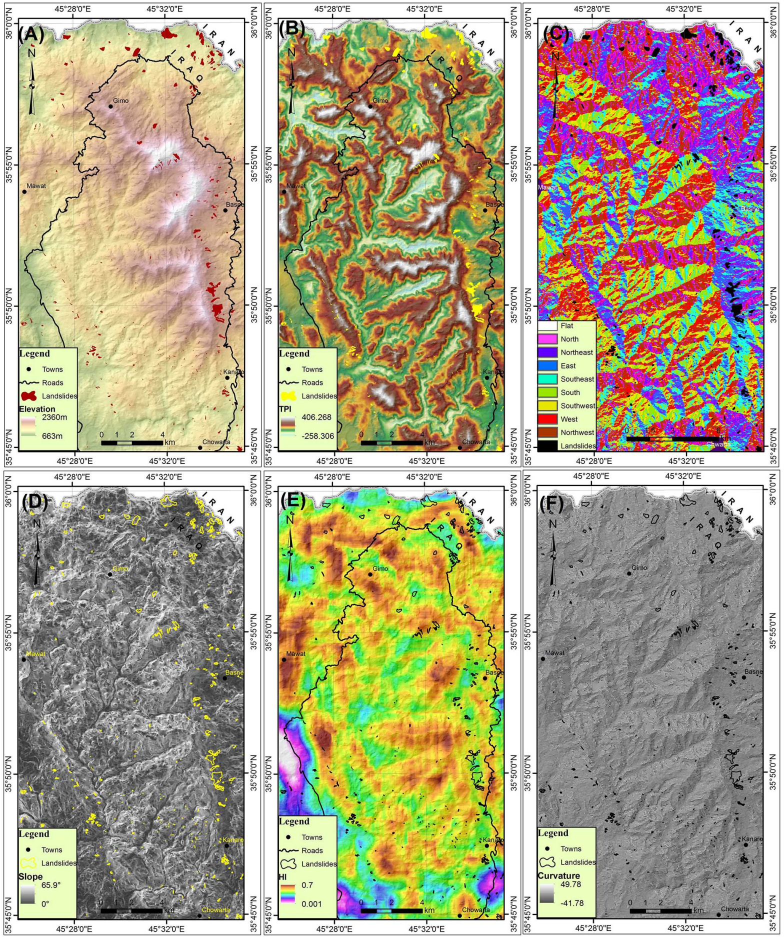

Figure 4. Maps of the landslide geomorphological prediction factors: **(a)** elevation; **(b)** TPI; **(c)** slope aspect; **(d)** slope angle; **(e)** HI; **(f)** curvature.

NHESSD
3, 1789–1833, 2015

Landslide susceptibility mapping in Mawat area, Kurdistan Region, NE Iraq

A. A. Othman et al.

Title Page
Abstract | Introduction
Conclusions | References
Tables | Figures
◂◂ | ▸▸
◂ | ▸
Back | Close
Full Screen / Esc
Printer-friendly Version
Interactive Discussion

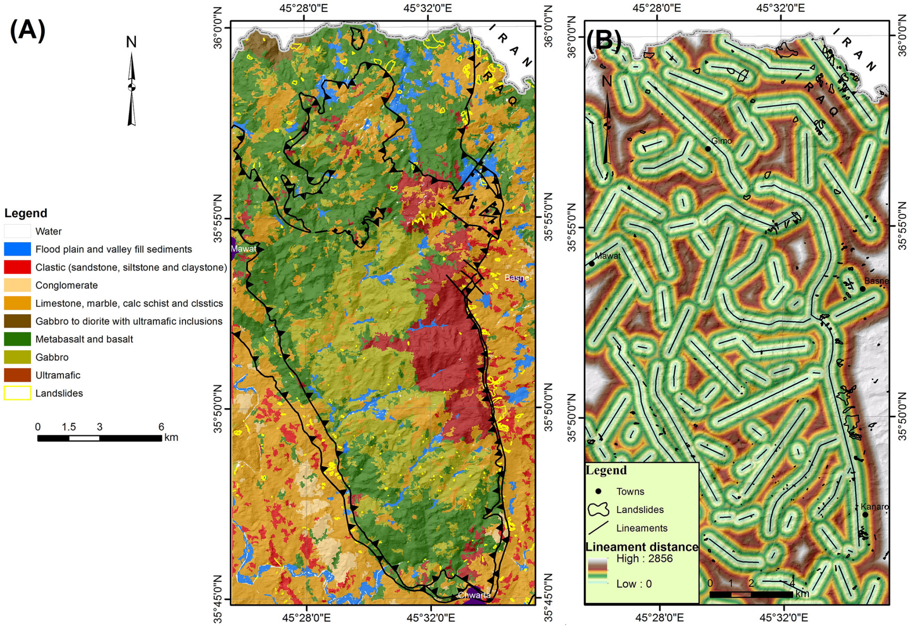

Figure 5. Maps of the landslide geological prediction factors: **(a)** lithology; **(b)** distance to lineaments.

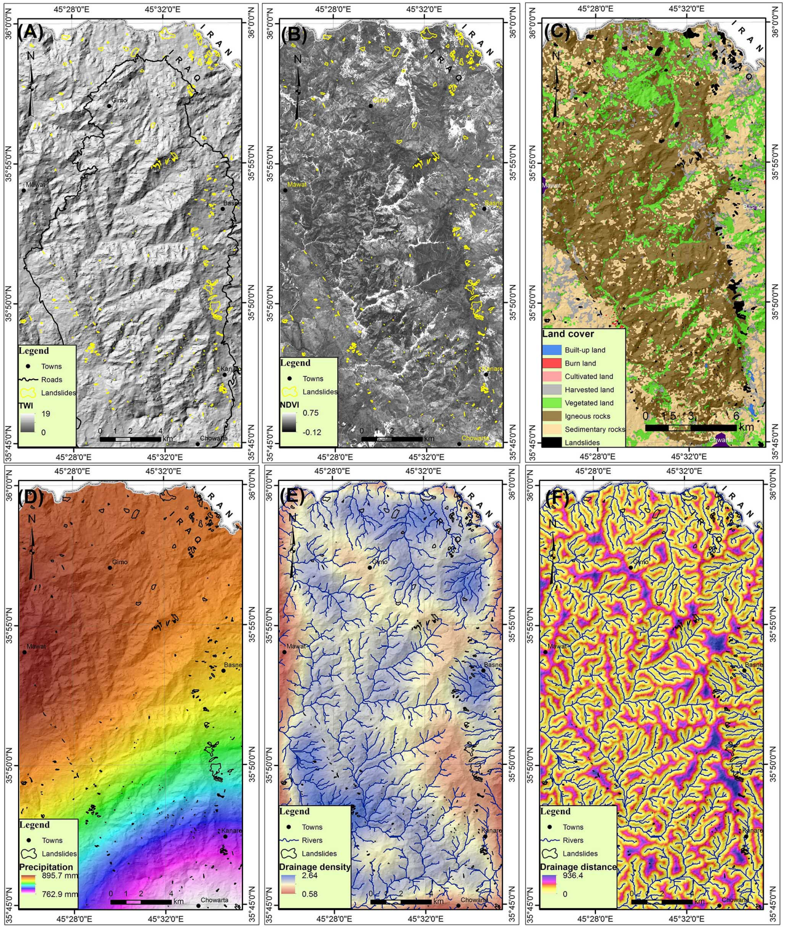

Figure 6. Maps of the landslide environmental prediction factors: **(a)** TWI; **(b)** NDVI; **(c)** land cover; **(d)** precipitation; **(e)** drainage density; **(f)** drainage distance.

NHESSD
3, 1789–1833, 2015

Landslide susceptibility mapping in Mawat area, Kurdistan Region, NE Iraq

A. A. Othman et al.

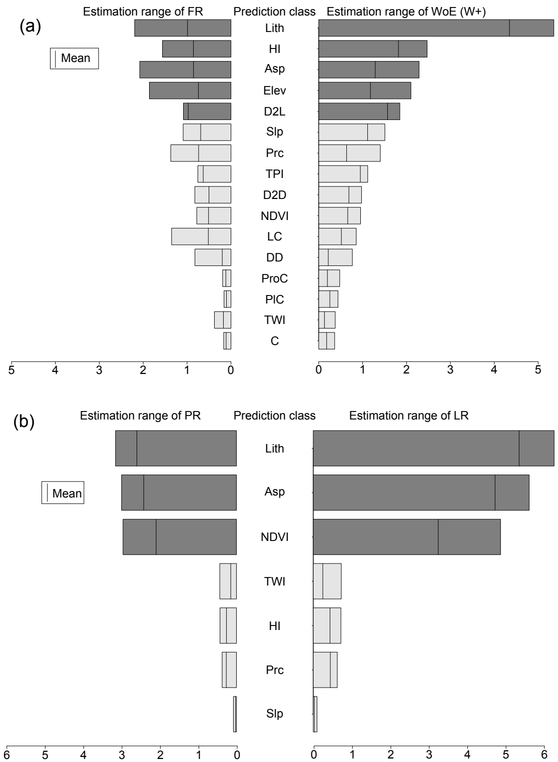

Figure 7. Pyramid plot shows the prediction factors estimation ranges of **(a)** weights of evidence and frequency ratio models **(b)** probit and logistic regressions models. Where, Lith is lithology, HI is hypsometric integral, Asp is aspect, Elev is elevation, D2L is distance to lineaments, Slp is slope, Prc = Precipitation, TPI is topographic position index, D2D is distance to drainage, NDVI is normalized difference vegetation index, LC is land cover, DD is drainage density, ProC is profile curvature, PlC is plan curvature, TWI is topographic wetness index, and C is curvature.

NHESSD
3, 1789–1833, 2015

Landslide susceptibility mapping in Mawat area, Kurdistan Region, NE Iraq

A. A. Othman et al.

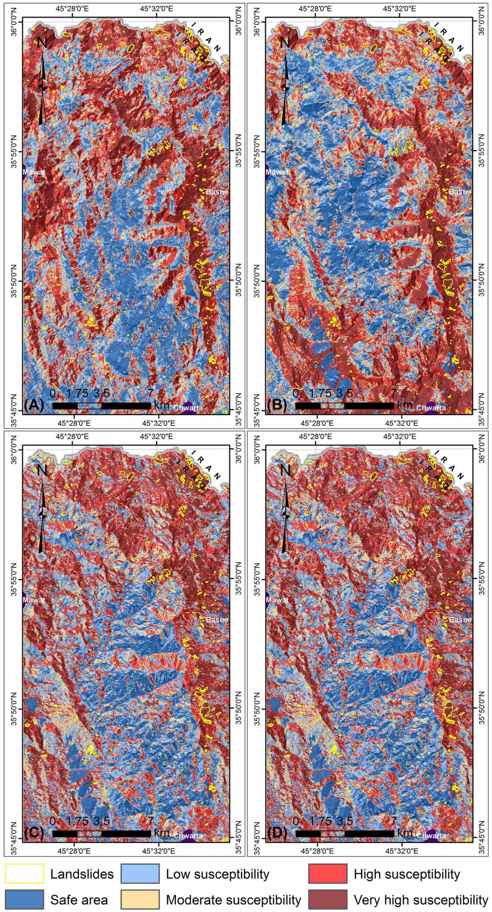

Figure 8. Best spatial distribution of the LSI of the study area based on different combinations models: **(a)** frequency ratio; **(b)** weights of evidence; **(c)** logistic regression; and **(d)** probit regression.

NHESSD

3, 1789–1833, 2015

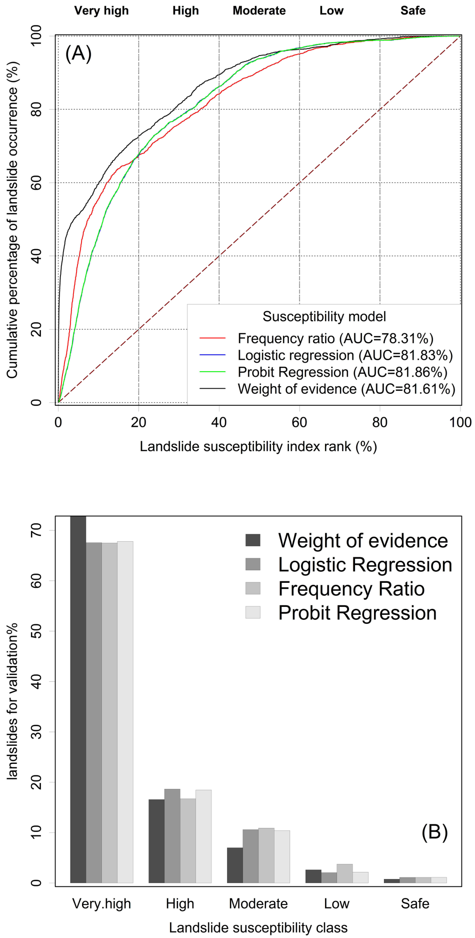

Figure 9. Bar graph showing **(a)** ROC curve evaluation of the four models. LR and PR curves gave similar results and are superimposed. **(b)** *R* index in different susceptibility classes.